ecule under study, we have calculated the frequencies of the four possible transitions for various molecules. Two pairs of close-lying lines result, and the calculated hyperfine splitting between these pairs (Table 1) agrees well with the experimental values given the underlying approximations.

Interestingly, both hyperfine components show up in the FDMR spectra, as is clear for molecules II and III in Fig. 4, in spite of the fact that we study single quantum systems. Apparently the triplet spin experiences both $^{13}$C nuclear spin configurations during the time (about 30 min) needed to accumulate the spectra. When the pentacene molecule is in $S_0$, the $^{13}$C nuclear spin can undergo energy conserving flip-flop transitions caused by the dipole-dipole interaction with other $^{13}$C nuclei. If the mean distance between two $^{13}$C nuclei is of the order of 10 nm, a rough estimate of this flip-flop time is 1 to 10 s, which is short relative to the accumulation time. We therefore observe a time average that is equivalent to the ensemble average according to the ergodic theorem.

For very small magnetic fields, the widths of the two hyperfine components for molecule II differ (see Fig. 4B). Each of the hyperfine components is built up by two transitions merged into one line. The width is caused by the hyperfine interaction with the 14 $^2$H nuclear spins. A calculation of this interaction shows that for $O_1$ molecules in very low fields the mixing of zero-field states is such that the second-order hyperfine interaction determines the linewidth of the low-frequency hyperfine component, whereas the first-order hyperfine interaction dominates for the high-frequency component. For a magnetic field of 7.5 mT, the hyperfine interaction becomes totally first-order and a more symmetrical pattern results. As seen for molecule III in Fig. 4C, this is already true at 3.8 mT for an $O_2$ molecule owing to the different orientation of the molecule with respect to the magnetic field.

## REFERENCES AND NOTES

1. W. E. Moerner and L. Kador, *Phys. Rev. Lett.* **62**, 2535 (1989).
2. M. Orrit and J. Bernard, *ibid.* **65**, 2716 (1990).
3. W. P. Ambrose and W. E. Moerner, *Nature* **349**, 225 (1991).
4. W. P. Ambrose, Th. Basché, W. E. Moerner, *J. Chem. Phys.* **95**, 7150 (1991).
5. A. Zumbusch, L. Fleury, R. Brown, J. Bernard, M. Orrit, *Phys. Rev. Lett.* **70**, 3584 (1993).
6. J. Bernard, L. Fleury, H. Talon, M. Orrit, *J. Chem. Phys.* **98**, 850 (1993).
7. Th. Basché, W. E. Moerner, M. Orrit, H. Talon, *Phys. Rev. Lett.* **69**, 1516 (1992).
8. W. E. Moerner and Th. Basché, *Angew. Chem. Int. Ed. Engl.* **32**, 457 (1993); M. Orrit, J. Bernard, R. I. Personov, *J. Phys. Chem.* **97**, 10256 (1993); W. E. Moerner, *Science* **265**, 46 (1994); A. B. Myers, P. Tchénio, M. Z. Zgierski, W. E. Moerner, *J. Phys. Chem.* **98**, 10377 (1994).
9. J. Köhler *et al.*, *Nature* **363**, 242 (1993).
10. J. Wrachtrup, C. von Borczyskowski, J. Bernard, M. Orrit, R. Brown, *ibid.*, p. 244.
11. J. Köhler, A. C. J. Brouwer, E. J. J. Groenen, J. Schmidt, *Chem. Phys. Lett.* **228**, 47 (1994).
12. J. Wrachtrup, C. von Borczyskowski, J. Bernard, M. Orrit, R. Brown, *Phys. Rev. Lett.* **71**, 3565 (1993).
13. P. J. L. Baudour, Y. Delugeard, H. Cailleau, *Acta Crystallogr. Sect. B* **32**, 150 (1976).
14. R. Brown, J. Wrachtrup, M. Orrit, J. Bernard, C. von Borczyskowski, *J. Chem. Phys.* **100**, 7182 (1994).
15. Th. Basché, S. Kummer, C. Bräuchie, *Chem. Phys. Lett.* **225**, 116 (1994).
16. T. T. Lin, J. L. Ong, D. J. Sloop, H. L. Yu, in *Pulsed EPR: A New Field of Applications*, C. P. Keijzers, E. J. Reijerse, J. Schmidt, Eds. (North-Holland, Amsterdam, 1989), p. 191.
17. H.-C. Fleischhauer, C. Kryschi, B. Wagner, H. Kupka, *J. Chem. Phys.* **97**, 1742 (1992); C. Kryschi, H.-C. Fleischhauer, B. Wagner, *Chem Phys.* **161**, 485 (1992).
18. SFS denotes the spectral roughness caused by the static, statistical number fluctuations of the emitting molecules.
19. We thank H. Zimmermann and H.-M. Vieth for providing pentacene-$d_{14}$. This work is supported by the Stichting voor Fundamenteel Onderzoek der Materie (FOM), with financial aid from the Nederlandse Organisatie voor Wetenschappelijk Onderzoek (NWO). One of us (J.K.) is fellow of the Human Capital and Mobility program of the European Community (grant ERBCHBICT920190).

2 February 1995; accepted 27 March 1995

# Electronic States in Gallium Arsenide Quantum Wells Probed by Optically Pumped NMR

R. Tycko,*† S. E. Barrett,*‡ G. Dabbagh, L. N. Pfeiffer, K. W. West

An optical pumping technique was used to enhance and localize nuclear magnetic resonance (NMR) signals from an *n*-doped GaAs/$Al_{0.1}Ga_{0.9}As$ multiple quantum well structure, permitting direct radio-frequency measurements of gallium-71 NMR spectra and nuclear spin-lattice relaxation rates ($1/T_1$) as functions of temperature (1.6 K $< T <$ 4.2 K) and the Landau level filling factor ($0.66 < \nu < 1.76$). The measurements reveal effects of electron-electron interactions on the energy levels and spin states of the two-dimensional electron system confined in the GaAs wells. Minima in $1/T_1$ at $\nu \approx 1$ and $\nu \approx 2/3$ indicate energy gaps for electronic excitations in both integer and fractional quantum Hall states. Rapid, temperature-independent relaxation at intermediate $\nu$ values indicates a manifold of low-lying electronic states with mixed spin polarizations.

Electrons in two-dimensional (2D) systems exhibit striking physical phenomena that are not observed in conventional 3D materials, particularly at low temperatures and in high magnetic fields. These phenomena include the integer quantum Hall effect (IQHE) and the fractional quantum Hall effect (FQHE) (*1*). The clearest realization of a 2D electron system (2DES) is provided by the conduction electrons in high-mobility semiconductor quantum wells, that is, thin layers of one semiconductor (here GaAs) embedded in thicker layers of a second *n*-doped semiconductor with a larger band gap (here delta-doped $Al_{0.1}Ga_{0.9}As$). Because of the band gap differences, the GaAs layers act as potential energy wells for the doped electrons and the $Al_{0.1}Ga_{0.9}As$ layers act as potential barriers. At low temperatures ($T \ll 100$ K), where only the lowest two dimensionally confined electron subband is populated, and in the absence of electron-electron interactions, the electronic properties of an ideal *n*-doped quantum well in a magnetic field $B$ can be understood in terms of the single-particle energy level diagram in Fig. 1 (*2*). The translational energy is quantized in Landau levels with splittings equal to the cyclotron energy $E_c = \hbar eB_z/m^*c$, where $\hbar$ is Planck's constant $h$ divided by $2\pi$, $e$ is the electron charge, $B_z$ is the component of the field normal to the plane of the wells, $m^*$ is the effective electron mass, and $c$ is the speed of light. The Landau levels are further split by the electron spin Zeeman energy $E_Z = g^*\mu_B|B|$, where $g^*$ is the effective $g$ value and $\mu_B$ is the Bohr magneton. Each energy level has well-defined values of the orbital ($N = 0, 1, 2, 3, \ldots$) and spin ($m = \pm 1/2$) quantum numbers and is highly degenerate, with degeneracy per unit area $n_B = eB_z/hc$. The Landau level filling factor is then defined as $\nu = n_s/n_B$, where $n_s$ is the conduction electron density per unit area in a single well, so that $\nu$ represents the number of spin-split Landau levels that are occupied at $T = 0$. The IQHE and FQHE refer to characteristic and universal plateaus in the Hall resistance and zeros in the longitudinal resistance of a 2DES at integral and certain fractional values of $\nu$. These effects, and other postulated phenomena such as Wigner crystallization, depend on deviations from the simple picture in Fig. 1

---

AT&T Bell Laboratories, 600 Mountain Avenue, Murray Hill, NJ 07974, USA.

*To whom correspondence should be addressed.

†Present address: National Institutes of Health, Building 5, Room 112, Bethesda, MD 20892, USA.

‡Present address: Department of Physics, Yale University, New Haven, CT 06520, USA.

caused by electron-electron Coulomb interactions and disorder (*1*).

The nature of the ground and excited electronic states in a real 2DES remains controversial, at least in part because of the limited range of experimental techniques (principally transport measurements) that have been applied to this problem. It was recently shown (*3*) that optical pumping [irradiation of interband transitions with near-infrared light (*4*)] enhances the nuclear spin polarizations, and hence the nuclear magnetic resonance (NMR) signals, in GaAs quantum wells at low temperatures by factors of 10 to 1000, allowing the direct detection of radio-frequency (rf) NMR signals from samples with multiple quantum wells. This result suggested that direct measurements of NMR frequency shifts and nuclear spin-lattice relaxation times ($T_1$), which are well-established probes of the electronic properties of bulk, 3D materials (*5*), might also prove to be useful experimental probes of 2DESs. We report here the results of optically pumped NMR (OPNMR) measurements of the dependence of the $^{71}$Ga nuclear spin-lattice relaxation rate ($1/T_1$) on $\nu$ and on $T$ in *n*-doped GaAs/$Al_{0.1}Ga_{0.9}As$ quantum wells. We observe signatures of both IQHE and FQHE states in these measurements. Our results demonstrate the importance of electron-electron interactions in determining the energies and spin states of a real 2DES.

A structure with multiple quantum wells, consisting of 40 GaAs wells 300 Å wide separated by $Al_{0.1}Ga_{0.9}As$ barriers 1800 Å wide, was grown by molecular beam epitaxy on a semi-insulating GaAs substrate. Silicon dopant atoms in the center of each barrier produced a carrier density $n_s = (1.41 \pm 0.14) \times 10^{11}$ cm$^{-2}$ in the wells with a mobility of $1.44 \times 10^6$ cm$^2$ V$^{-1}$ s$^{-1}$, as determined by low-field transport measurements at 4.2 K. Samples for OPNMR measurements were approximately 1.0 cm by 0.5 cm. Measurements were made in fields of 7.05 and 9.39 T ($^{71}$Ga NMR frequencies of 91.6 and 121.8 MHz, respectively) and at temperatures between 1.6 and 4.2 K. Optical pumping was performed with circularly polarized light ($\sigma+$, 10 to 800 mW cm$^{-2}$, 805.5-nm wavelength) from a laser diode array, gated by a shutter under control of the NMR spectrometer. We varied $\nu$ at constant $B$ by tilting the sample. Using a single-axis goniometer, we could set the angle $\theta$ between $B$ and the direction normal to the plane of the wells from 0° to 60° with an accuracy of roughly ±0.5°; $\nu$ is then proportional to $(\cos \theta)^{-1}$.

The experimental timing sequence is shown in Fig. 2A. After a train of rf pulses that destroys any residual nuclear spin polarization, the laser shutter opens for a time $\tau_L$. The shutter then closes for a time $\tau_D$ before a single rf pulse is applied to excite the NMR free-induction-decay signals. When the OPNMR signals are observed in the dark, the spectra and relaxation rates represent properties of the system at thermal equilibrium.

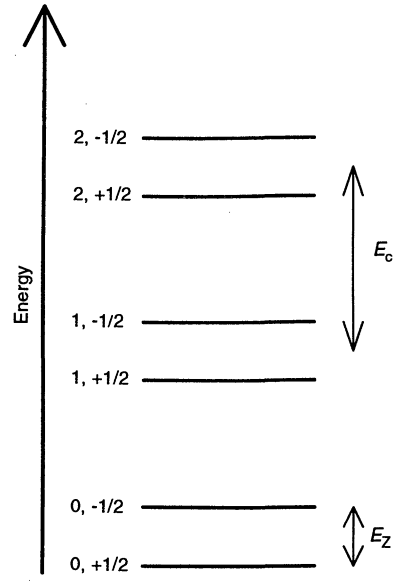

**Fig. 1.** Single-particle energy levels for an ideal noninteracting, two-dimensionally confined electron system in a magnetic field, showing the cyclotron energy ($E_c$) and Zeeman energy ($E_Z$) splittings and the orbital ($N$ = 0,1,2,3, . . .) and spin ($m$ = ±1/2) quantum numbers. In the experiments described here, $E_c$ ~15 meV and $E_Z$ ~0.2 meV.

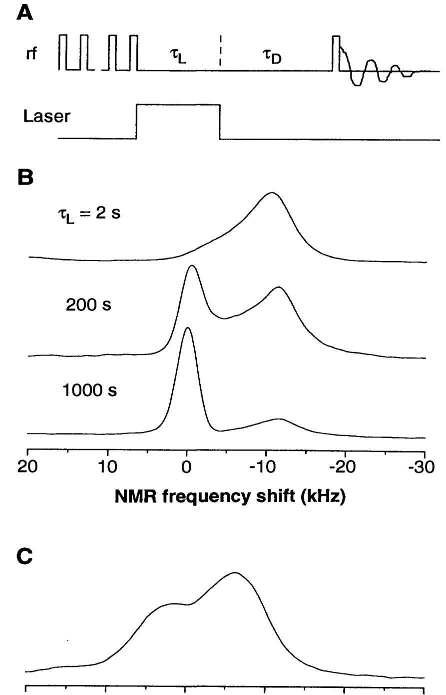

**Fig. 2.** (**A**) Timing diagram for optically pumped NMR measurements. (**B**) The $^{71}$Ga NMR spectra at 1.9 K, 7.05 T, and $\nu$ = 0.88 ($\theta$ = 0°), with $\tau_D$ = 1 s and indicated values of $\tau_L$ (200-mW light). The spectrum at $\tau_L$ = 2 s is the result of 32 scans; the spectra at $\tau_L$ = 200 s and $\tau_L$ = 1000 s are the results of single scans. Vertical scales are arbitrary. (**C**) Spectrum obtained with $\tau_L$ = 2 s and with the laser shutter open during acquisition of the NMR signals, showing the light-induced shift and broadening of the signal from nuclei in the GaAs wells.

Figure 2B shows typical $^{71}$Ga OPNMR spectra obtained with $\tau_D$ fixed at 1 s. For small values of $\tau_L$, a single asymmetric resonance line is observed. For larger values of $\tau_L$, a second, narrower and symmetric line appears at higher frequency. With increasing $\tau_L$, the total NMR signal intensity increases and the narrow line becomes dominant. Although the NMR lines are plotted in the conventional upward direction, they are emissive, as observed in earlier OPNMR measurements (*3*). Because the optical pumping wavelength was chosen so that light is absorbed and nuclear spin polarization is generated only in the wells, the lower frequency resonance must be assigned to $^{71}$Ga nuclei in the GaAs wells. We assign the higher frequency resonance to $^{71}$Ga nuclei in the $Al_{0.1}Ga_{0.9}As$ barriers. The barrier signal grows as nuclear spin polarization diffuses from $^{71}$Ga nuclei in the wells to $^{71}$Ga nuclei in the barriers during $\tau_L$. This nuclear spin diffusion is driven by nuclear magnetic dipole-dipole couplings (*6*) and is accelerated by the fact that the well signal shifts to higher frequency and overlaps the barrier signal during optical irradiation (Fig. 2C). The spectra in Fig. 2 illustrate both the sensitivity and the spatial selectivity achievable with OPNMR.

We attribute the frequency shift $\Delta f$ between the well and the barrier signals to the magnetic hyperfine coupling between $^{71}$Ga nuclei and doped electrons in the wells (*7*).

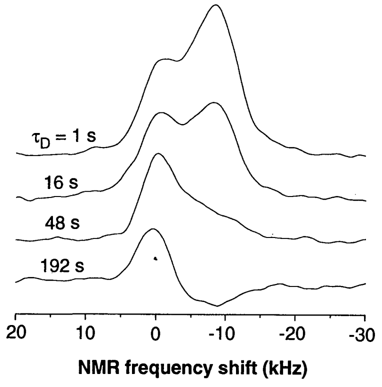

**Fig. 3.** The $^{71}$Ga NMR spectra at 2.1 K, 9.39 T, and $\nu$ = 1.20 ($\theta$ = 56.7°), with $\tau_L$ = 10 s and indicated values of $\tau_D$. Vertical scales are the same for all spectra. Each spectrum is the result of a single scan. The dependence on $\tau_D$ is due primarily to nuclear spin-lattice relaxation in the GaAs wells.

Because the electronic wave functions at the GaAs conduction band edge are constructed from *s* orbitals (8), the hyperfine coupling is primarily a Fermi contact (isotropic) interaction (7, 9) and $\Delta f = A\rho(z)\langle S_{z'}\rangle$, where $A$ is a coupling constant, $\rho(z)$ is the conduction electron density envelope function, $z$ is the displacement of the nucleus in the direction normal to the plane of the well, and $\langle S_{z'}\rangle$ is the expectation value of the electron spin angular momentum along the field direction $z'$. The observed NMR frequency shift is therefore a measure of the spin polarization of the 2DES. The asymmetric line shape of the well results from the fact that $\rho(z) \approx \rho_{\max} \sin^2(\pi z/w)$ within a well of width $w$ ($0 < z < w$) and the fact that optical pumping creates nuclear spin polarization preferentially near $z = w/2$. The dependence of $\Delta f$ on $\nu$ and $T$ is considered in detail elsewhere (9).

Figure 3 shows a series of $^{71}$Ga OPNMR spectra obtained with $\tau_L$ fixed at 10 s and increasing values of $\tau_D$. Signal intensity from the wells decreases with increasing $\tau_D$ and eventually inverts (that is, becomes absorptive), whereas intensity from the barriers remains nearly constant. In principle, these intensity changes are due to a combination of nuclear spin-lattice relaxation, which tends to return the nuclear spin polarization to its thermal equilibrium value with a time constant $T_1$ that depends on $z$, and nuclear spin diffusion, which tends to produce a uniform nuclear spin polarization throughout the quantum well structure. However, the fact that the barrier signal changes very slowly relative to the well signal indicates that spin diffusion between wells and barriers becomes negligible when the shutter is closed and the spectral overlap is reduced (6). Moreover, $T_1$ must be much smaller in the wells than in the barriers, implying that nuclear spin-lattice relaxation in the wells is driven by hyperfine coupling to the doped electrons (10).

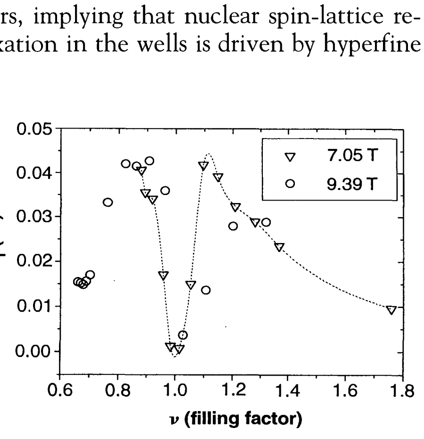

**Fig. 4.** Spin-lattice relaxation rate ($1/T_1$) for $^{71}$Ga nuclei in GaAs wells at 2.1 K as a function of the Landau level filling factor $\nu$. The dashed line is a guide to the eye drawn through data acquired at 7.05 T. Standard deviations were approximately ±10% for the largest values of $1/T_1$ and approximately ±25% for the smallest values.

Figure 4 shows the experimental dependence of $1/T_1$ in the wells on $\nu$ at 2.1 K. We determined $T_1$ from OPNMR spectra as in Fig. 3 by fitting the signal intensity at the peak frequency in the well line shape to the form

$$S(\tau_D) = S_0 \exp(-\tau_D/T_1) + S_1 \quad (1)$$

which describes the data to within the experimental noise. Values of $\nu$ are calculated with $n_s = 1.50 \times 10^{11}$ cm$^{-2}$, corresponding to $\nu = 1$ at $\theta = 28.5°$ in a 7.05-T field and $\theta = 48.7°$ in a 9.39-T field. With this value of $n_s$, maxima in $\Delta f$ occur at $\nu = 1.00 \pm 0.03$ in both fields (9). Several features of the data in Fig. 4 are significant. First, nuclear spin-lattice relaxation becomes very slow ($T_1 > 250$ s) at $\nu \approx 1$ in both the 9.39-T and the 7.05-T fields. Second, relaxation is rapid ($T_1 \approx 24$ s) on either side of $\nu = 1$. A change in $\theta$ of only 3° can produce a 20-fold change in the relaxation rate. Third, an apparent minimum in $1/T_1$ also occurs at $\nu \approx 2/3$, corresponding to a FQHE state. The striking similarity of the dependences of $1/T_1$ on $\nu$ (rather than on $\theta$) in different fields implies that nuclear spin-lattice relaxation is mediated by the Fermi contact part of the hyperfine coupling and that the relaxation data reflect the dependence of the electronic state on $\nu$.

The temperature dependence of $1/T_1$ in the wells is shown in Fig. 5. Within experimental precision, $1/T_1$ is temperature-independent at $\nu = 0.88$ between 1.6 K and 4.2 K; $1/T_1$ is strongly temperature-dependent at $\nu \approx 1$ and $\nu \approx 2/3$.

Nuclear spin-lattice relaxation due to a Fermi contact hyperfine interaction $H_h$ in a solid (7) is a scattering process in which the electron system makes a transition between initial and final many particle states $|i\rangle$ and $|f\rangle$, with energies $E_i$ and $E_f$, respectively, and simultaneously the $z'$ component of nuclear spin angular momentum changes from $p\hbar$ to $(p\pm1)\hbar$. The rate is then

$$\frac{1}{T_1} \propto \sum_{i,f} |\langle f,p\pm1|H_h|i,p\rangle|^2 \times e^{-E_i/kT}\delta(E_i - E_f \mp \hbar\omega_n) \quad (2)$$

($k$ is Boltzmann's constant). Because the nuclear Zeeman energy $\hbar\omega_n \sim 4 \times 10^{-4}$ meV, $|i\rangle$ and $|f\rangle$ must be nearly degenerate to contribute to $1/T_1$. Because the Fermi contact interaction conserves total spin angular momentum, $|i\rangle$ and $|f\rangle$ must also differ by one electron spin flip. If the noninteracting electron picture in Fig. 1 were strictly valid, there would be no states $|i\rangle$ and $|f\rangle$ that satisfy both criteria. Nuclear spin-lattice relaxation would necessarily result from other, weaker mechanisms and would be very slow at all values of $\nu$, in obvious disagreement with our experimental measurements.

The difficulty in explaining rapid nuclear spin-lattice relaxation in a 2DES has been recognized, particularly in the context of earlier, indirectly detected measurements of $T_1$ in an *n*-doped GaAs quantum well by Berg *et al.* (11–15). In these earlier experiments, a composite relaxation rate for all nuclei in a GaAs well (in contrast to our measurements of $T_1$ for a single isotope) was found to be an oscillating function of $\nu$ at 1.3 K for $2 \lesssim \nu < 4$, with broad minima at integral $\nu$ and $200\ \text{s} < T_1 < 1200$ s. Berg *et al.* (11) and Iordanskii *et al.* (12) explained these results within the single-particle picture in Fig. 1 by invoking a broadening of the Landau levels (resulting from disorder) and a $\nu$-dependent enhancement of $E_c$ (caused by electron-electron exchange interactions), so that electronic states with the same $N$ but different $m$ could overlap in energy in a $\nu$-dependent way. Antoniou and MacDonald (13) pointed out that proper inclusion of Landau level broadening and exchange enhancement of $E_c$ could lead to either broad minima or broad maxima at integral $\nu$, depending on the degree of disorder. Existing theories of nuclear spin-lattice relaxation in 2DESs (11–15) also predict a strong temperature dependence of $T_1$ at all values of $\nu$. The data in Figs. 4 and 5 cannot be explained by existing theories.

We explain the data in Figs. 4 and 5 by referring to the many-particle energy level schemes in Fig. 6. At $\nu = 1$, there is a

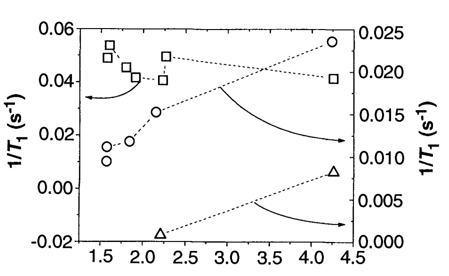

**Fig. 5.** Temperature dependence of the $^{71}$Ga spin-lattice relaxation rate at $\nu = 0.88$ (squares, $\theta = 0°$, 7.05 T, left scale), $\nu = 0.67$ (circles, $\theta = 10°$, 9.39 T, right scale), and $\nu = 1.01$ (triangles, $\theta = 30°$, 7.05 T, right scale). Dashed lines are guides to the eye.

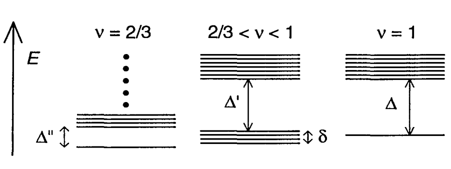

**Fig. 6.** Schematic many-particle energy level diagrams for the two-dimensionally confined electron system in the GaAs wells at the indicated Landau level filling factors, as suggested by the nuclear spin-lattice relaxation data.

single, spin-polarized electronic ground state, separated from all excited states by an energy gap $\Delta$, with $\Delta \gg 0.1$ meV (the thermal energy $kT$ at 1.2 K). Nuclear spin-lattice relaxation can occur only in the excited states, making $1/T_1$ small and temperature-dependent. For $2/3 < \nu < 1$, there is a manifold of low-energy electronic states, with energy width $\delta$. These states have varying degrees of electron spin polarization, so that nuclear spin relaxation can take place rapidly within the low-energy manifold [and $\Delta f$ is smaller than at $\nu = 1$, as observed (9)]. If $\delta < 0.1$ meV and $\Delta' \gg 0.1$ meV, $1/T_1$ will be nearly temperature-independent over the range of our measurements (16). At $\nu = 2/3$, there is again a single electronic ground state, separated from higher energy states by $\Delta''$. If $\Delta'' \gtrsim 0.1$ meV, $1/T_1$ is again relatively small and temperature-dependent (17). The reduced spin polarization of the low-energy states for $2/3 < \nu < 1$ (and of the excited states), the energy gap $\Delta''$, and the energy width $\delta$ are consequences of electron-electron interactions. This picture of the many particle states is generally consistent with transport measurements (1, 18), which show $\Delta'' \approx$ 0.1 to 0.5 meV at $\nu = 2/3$ and 9.39 T, and calculations (19), which suggest that the spin polarization of the low-energy states at $\nu = 1 \pm \varepsilon$ is strongly reduced by electron-electron interactions. Our results show that, in a real 2DES, there exist nearly degenerate electronic states with different values of $\langle S_{z'} \rangle$ and suggest that the energy gaps for electronic spin excitations at $\nu = 2/3$ and $\nu = 1$ are similar to the energy gaps for charge excitations.

A more quantitative understanding of the energy splittings and spin polarizations is to be expected from additional OPNMR measurements. Although samples with multiple quantum wells were used in the experiments reported here, the OPNMR signals from the wells are sufficiently strong and resolved from barrier and substrate signals that similar measurements on single quantum wells ($\lesssim 10^{16}$ $^{71}$Ga nuclei) should be possible.

## REFERENCES AND NOTES

1. J. T. Devreese and F. M. Peeters, *The Physics of the Two-Dimensional Electron Gas* (Plenum, New York, 1987); J. P. Eisenstein and H. L. Stormer, *Science* **248**, 1510 (1990); J. K. Jain, *ibid.* **266**, 1199 (1994).
2. C. Weisbuch and B. Vinter, *Quantum Semiconductor Structures* (Academic Press, San Diego, 1991), pp. 123–139.
3. S. E. Barrett, R. Tycko, L. N. Pfeiffer, K. W. West, *Phys. Rev. Lett.* **72**, 1368 (1994).
4. G. Lampel, *ibid.* **20**, 491 (1968); D. Paget, G. Lampel, B. Sapoval, V. I. Safarov, *Phys. Rev. B* **15**, 5780 (1977); G. P. Flinn, R. T. Harley, M. J. Snelling, A. C. Tropper, T. M. Kerr, *Semicond. Sci. Technol.* **5**, 533 (1990); V. K. Kalevich, V. L. Korenev, O. M. Fedorova, *JETP Lett.* **52**, 349 (1990); M. Krapf, G. Denninger, H. Pascher, G. Weimann, W. Schlapp, *Solid State Commun.* **78**, 459 (1991); S. K. Buratto, D. N. Shykind, D. P. Weitekamp, *Phys. Rev. B* **44**, 9035 (1991); *J. Vac. Sci. Technol. B* **10**, 1740 (1992).
5. For recent examples, see: R. Tycko, *J. Phys. Chem. Solids* **54**, 1713 (1993); R. Tycko *et al.*, *Science* **253**, 884 (1991); R. E. Walstedt and W. W. Warren Jr., *ibid.* **248**, 1082 (1990); J. A. Martindale *et al.*, *Phys. Rev. Lett.* **68**, 702 (1992).
6. D. Suter and R. R. Ernst, *Phys. Rev. B* **32**, 5608 (1985); R. Tycko and G. Dabbagh, *Isr. J. Chem.* **32**, 179 (1992).
7. J. Winter, *Magnetic Resonance in Metals* (Oxford Univ. Press, London, 1971).
8. S. L. Richardson, M. L. Cohen, S. G. Louie, J. R. Chelikowsky, *Phys. Rev. B* **33**, 1177 (1986).
9. S. E. Barrett, G. Dabbagh, L. N. Pfeiffer, K. W. West, R. Tycko, *Phys. Rev. Lett.*, in press.
10. Numerical simulations of the dependence of the OPNMR spectra on $\tau_D$, based on the equation
$$\frac{\partial p}{\partial t} = D \frac{\partial^2 p}{\partial z^2} - \frac{1}{T_1(z)} (p - p_{eq})$$
for the nuclear spin polarization $p(z,t)$ with $T_1(z) \propto \rho(z)^{-2}$, indicate that the effective diffusion constant $D$ for nuclear spin diffusion between wells and barriers is less than 10 Å$^2$ s$^{-1}$ for all $\nu$ under our experimental conditions. Spin diffusion reduces the apparent $T_1$ for well nuclei by less than 10%.
11. A. Berg, M. Dobers, R. R. Gerhardts, K. v. Klitzing, *Phys. Rev. Lett.* **64**, 2563 (1990).
12. S. V. Iordanskii, S. V. Meshkov, I. D. Vagner, *Phys. Rev. B* **44**, 6554 (1991).
13. D. Antoniou and A. H. MacDonald, *ibid.* **43**, 11686 (1991).
14. Y. N. Ovchinnikov, I. D. Vagner, A. M. Dyugaev, *JETP Lett.* **59**, 569 (1994).
15. J. H. Kim, I. D. Vagner, L. Xing, *Phys. Rev. B* **49**, 16777 (1994).
16. In principle, particular combinations of the many-particle density of states and the matrix elements $\langle f, p \pm 1 | H_h | i, p \rangle$ could give rise to a temperature-independent $1/T_1$ without requiring an energy gap. This seems an unlikely possibility.
17. An excitation energy gap is also expected at $\nu = 4/3$. The corresponding minimum in $1/T_1$ is not apparent in Fig. 4 either because the data points are too widely spaced or because the gap is significantly smaller than that at $\nu = 2/3$.
18. G. S. Boebinger, A. M. Chang, H. L. Stormer, D. C. Tsui, *Phys. Rev. Lett.* **55**, 1606 (1985); J. E. Furneaux, D. A. Syphers, A. G. Swanson, *ibid.* **63**, 1098 (1989).
19. S. L. Sondhi, A. Karlhede, S. A. Kivelson, E. H. Rezayi, *Phys. Rev. B* **47**, 16419 (1993); H. A. Fertig, L. Brey, R. Côté, A. H. MacDonald, *ibid.* **50**, 11018 (1994).

18 January 1995; accepted 20 March 1995

---

# Monodisperse Metal Clusters 10 Angstroms in Diameter in a Polymeric Host: The "Monomer as Solvent" Approach

Josh H. Golden, Haibin Deng, Francis J. DiSalvo,
Jean M. J. Fréchet,* Patrick M. Thompson

A general methodology is presented for the dispersion of an inorganic compound within an organic polymer host through the use of solubilizing and polymerizable ligands. The dispersion of metal cluster cations 10 angstroms in diameter within a polymer host is achieved by free-radical polymerization of the hexafunctional metal cluster $[Mo_6Cl_8(NVI)_6](triflate)_4$ with bound polymerizable ligands in *N*-vinylimidazole (NVI) solutions. Copolymerization of the activated cluster-bound ligands with the surrounding medium probably plays a key role in preventing aggregation and produces near monodisperse molecular clusters within the polymer matrix.

Intense research efforts are now being focused on the design and fabrication of materials that contain metal nanoclusters (1 to 10 nm) because of real and potential applications of these materials in optics and electronics (1). Nanoscale metal clusters display a variety of useful physical properties including catalysis (1, 2), magnetism (3), and size-dependent light absorption (the quantum size effect) (1, 4, 5). A major challenge in the preparation of these materials is the prevention of both phase separation and aggregation of the clusters within the host matrix. Strategies used to control cluster aggregation, size, and morphology include the electrochemical synthesis of surfactant-stabilized clusters (1), in situ formation of metal clusters in the polar segments of diblock copolymers (5), and metal vapor deposition (1, 6). We now report a general methodology for the preparation of near monodisperse nanoclusters in a polymer host by cluster copolymerization with a solubilizing monomer-solvent medium.

Our strategy, termed the "monomer as solvent" approach, involves the design of a monomer that can act as both a ligand and a solvent for the metal nanoclusters. In this approach, phase separation is not expected because the vinyl-functionalized clusters are an integral part of the polymerization system. In effect, they act as the loci for cross-linking of the surrounding dispersing medium. To achieve this goal, it is first necessary to identify a polar organic solvent that also acts as a ligand. Structurally related mono-

---

J. H. Golden, H. Deng, F. J. DiSalvo, J. M. J. Fréchet, Department of Chemistry, Baker Laboratory, Cornell University, Ithaca, NY 14853, USA.
P. M. Thompson, Eastman Kodak Company, Rochester, NY 14650, USA.

*To whom correspondence should be addressed.